ESIC2024, Vol 8.2, S2 Posted: 04/08/2024

Experimental Research on the Degradation of Mechanical Properties and Microstructural Evolution of Ultra-High-Performance Concrete Under Fire Conditions

Ngoc-Vinh Nguyen[1], Su Su Phyo Thu[1], Nguyen Van Thanh[2], Pham Huy Hoa[2], Hoang Van Dat[2], Nguyen Dinh Duc[2]

[1]Faculty of Advanced Technology and Engineering, VNU Vietnam Japan University, Vietnam,
[2]Faculty of Civil Engineering – VNU Hanoi, University of Engineering and Technology, Vietnam
Email: nn.vinh@vju.ac.vn

Abstract

Ultra-high-performance concrete (UHPC) is gaining popularity due to its superior mechanical properties, including high strength, toughness, durability, and excellent seismic performance. However, the risk of explosive spalling in UHPC structures exposed to fire poses a significant challenge, fundamentally hindering comprehensive studies on fire safety and limiting the broader engineering applications of UHPC. In this study, the mixture proportion of UHPC was developed and optimized by comparing the usage of yellow river and standard sands, different types of chemical admixtures, and different curing regimes. Furthermore, a sensitive case study was also conducted to optimize the calcined bauxite content to improve UHPC's fire resistance. For these purposes, 189 UHPC cubes, incorporating variations in particle types, superplasticizer types, and curing regimes, were tested under three thermal levels, such as 200℃,400℃, and 600℃. The microstructural evolution of heated cube specimens was then observed using a scanning electron microscope (SEM) examination. Calcined bauxite was then considered to replace the standard sand to improve the fire resistance of UHPC and enhance the residual compressive strength of cube specimens under thermal conditions. For this purpose, 0%, 20%, 40%, 60%, 80%, and 100% calcined bauxite content was designed as six case studies. Furthermore, the degradation of UHPC strength was also investigated for the corresponding six case studies by conducting the uniaxial compressive experiments. Finally, the microstructural evolution under both thermal conditions and calcined bauxite content was observed and discussed.

Keywords: Explosive spalling; Fire Resistance; Microstructure; Spalling Behavior; Ultra-High-Performance Concrete.

1. Introduction

Ultra-high-performance concrete (UHPC) has emerged as a promising construction material with exceptional mechanical properties, exceeding conventional concrete's by a significant margin. Its high compressive strength, tensile strength, and ductility make it well-suited for various structural applications, such as bridges, tunnels, and high-rise buildings [1–6]. This remarkable performance stems from its unique composition, which includes a carefully balanced blend of high-quality cement, fine aggregates, silica fume, and steel fibers [1,7–9]. UHPC's high strength-to-weight ratio enables more slender and efficient structural designs, reducing material consumption and minimizing construction weight, thereby making it a sustainable choice for building construction [7]. However, a significant challenge to its widespread adoption is its susceptibility to fire-induced spalling, which can severely compromise the structural integrity and safety of UHPC structures [10]. Exposure to fire can significantly reduce the compressive strength, flexural strength, and modulus of elasticity of UHPC, highlighting the necessity to improve its fire resistance for broader application in buildings and infrastructure[11–13].

Spalling, a critical concern for UHPC under thermal conditions, is characterized by the explosive detachment of concrete fragments [10,14–16]. This phenomenon is primarily triggered by the buildup of internal vapor pressure and thermal stress within the concrete during exposure to fire [10]. The dense microstructure and low permeability of UHPC hinder the release of moisture generated as it heats up, contributing to this vulnerability [10]. To address this critical issue, numerous studies have focused on enhancing the fire resistance of UHPC by incorporating various mitigation strategies, including steel fibers, polypropylene fibers, and hybrid combinations [17–19]. While these approaches have proven effective in reducing or preventing spalling, the search for more sustainable and cost-effective solutions remains ongoing.

Currently, the strategies to mitigate the spalling behavior in UHPC include the incorporation of polypropylene (PP) fibers. PP fibers, which melt at elevated temperatures, enhance the permeability of the UHPC matrix, facilitating steam escape and reducing pore pressure to prevent spalling [17]. Recent studies by Du et al. (2020) have demonstrated the effectiveness of this approach, emphasizing the significance of selecting fibers with suitable thermal properties. This contrasts with the findings of Zhang et al. (2021), who investigated the incorporation of polyethylene (PE) fibers [16,18]. Although PP fibers have proven effective in preventing spalling, further research is necessary to understand the optimal fiber dosage, type, and distribution for various UHPFRC compositions and structural configurations. Missemer et al. (2019) [14] pointed out that small polypropylene (PP) fibers were more effective in resisting fire spalling than acrylic fibers. Their blowtorch tests revealed that fiber geometry and concentration significantly impacted spalling behavior, and the researchers proposed a new “critical factor” (Fzc) based on pore size distribution as a more reliable predictor of spalling resistance.

Another approach to mitigate the spalling behavior in UHPC is the usage of calcined bauxite (CB), which is attributed to a readily available and cost-effective material and derived from bauxite ore through high-temperature calcination. This material has been extensively studied for its diverse applications, particularly in the construction industry. Previous research has demonstrated the potential of calcined bauxite aggregates to improve the fire resistance of various materials, including asphalt mixtures and castables [20–22]. The calcined bauxite in the

concrete mixture can influence thermal conductivity and heat transfer behavior, contributing to a more even temperature distribution and reduced thermal stress during fire exposure. This leads to the reduction of the spalling risk by controlling temperature gradients within the material. The inherent properties of calcined bauxite make it a promising candidate for enhancing the fire resistance of UHPC. Its high alumina content (AL_2O_3) contributes to improved thermal stability, while its specific mineral composition, including corundum and mullite, promotes heat resistance and reduces spalling [22]. Moreover, its lightweight nature can reduce the overall thermal mass of UHPC, mitigating heat transfer and minimizing temperature gradients within the concrete structure. Geopolymers made from calcined bauxite and ground-granulated blast furnace slag exhibit improved thermal stability compared to traditional geopolymers [23]. Guan et al. (2023) [20] investigated the use of magnetite (MT) in combination with calcined bauxite in high-friction surface treatment (HFST) for pavement applications. The experimental results demonstrated that MT significantly enhanced microwave absorption and deicing efficiency, contributing to improved winter road safety. S. Li et al., (2021) examined the influence of calcined bauxite aggregates' chemical composition on their mechanical and physical properties, emphasizing the significant impact of (AL2O3) content on polish resistance, adhesion, and bulk density. This study highlighted the importance of bauxite's chemical composition for optimizing the performance of high-friction surface courses [22].

Zhong & Zhang (2023) investigated using fine calcined bauxite aggregate (CBA) in cementitious matrices to improve projectile impact resistance. Their finding suggests that using CBA is more effective than employing organic admixtures in reducing penetration depth and enhancing impact resistance. While the study focuses on impact resistance, the potential of CBA to improve the structural integrity of concrete could translate into enhanced fire resistance, as a stronger matrix is better equipped to withstand thermal stresses and cracking [24]. While significant progress has been made in mitigating spalling and improving fire resistance, several limitations and new issues require further investigation. Most studies focus on specific applications like refractory concrete, high-friction surface courses, or impact resistance. Although these studies provide valuable insights into the potential of bauxite in various applications, the influences of thermal conditions and CB content on the residual compressive strength and microstructural evolution of UHPC have not been well studied.

This study aims to optimize the usage of particles, such as yellow river and ISO standard sands, different chemical admixtures, and curing regimes. The influences of CB contents on residual compressive strength and microstructural evolution were also investigated and discussed. Finally, the degradation of mechanical properties of UHPC under fire conditions was clarified. The findings of this study provide a further understanding of the fire performance of bauxite-based UHPC, leading to safer and more sustainable construction practices.

2. Experiments on UHPC

Materials and mixture design

In this study, a series of experiments, including uniaxial compressive, spalling tests, and a scanning electron microscope (SEM) examination, was adapted to investigate the spalling

severity, the degradation of mechanical properties as well as the microstructural evolution of UHPC under thermal conditions. In total, 189 UHPC cube specimens corresponding to six case studies of bauxite replacement ranging from 0% to 100%, in which 72 specimens will be used for the spalling tests under different thermal conditions, such as 200°C, 400°C, 600°C, and 800°C. Standardized specimen preparation, curing procedures, and fire exposure protocols will be meticulously followed to ensure consistency and control. Compressive strength, spalling severity, and microstructural changes (pore structure, crack formation, and elemental composition) will be assessed.

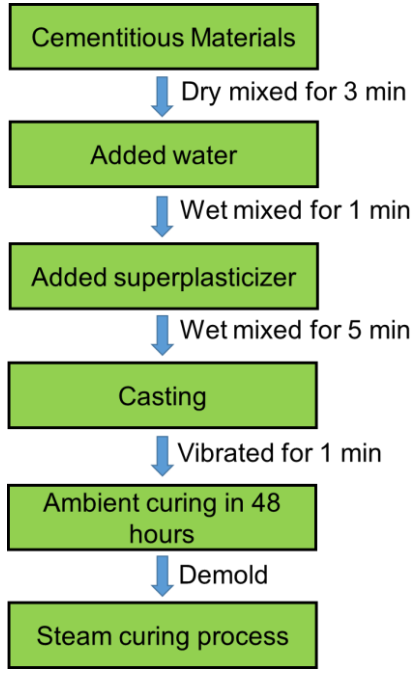

Fig. 1. UHPC casting flowchart.

The UHPC composition included cement, silica fume, silica sand, silica powder, superplasticizer, water, and bauxite (calcined form) as listed in Table 1. The purpose was to investigate the microstructural evolution and residual strength of UHPC under thermal conditions. To control the rotation speed, a 20-liter laboratory mixer was employed to prepare the UHPC specimens as pointed out in [25–27]. A 10 μm average diameter of silica powder, a 0.1 μm average diameter of silica fume, and a 1.0 mm maximum diameter of silica sand were employed in this study. Both silica fume and silica powder have a SiO2 content exceeding 98%. The cementitious materials (cement, silica fume, silica sand, silica powder, and bauxite) were initially mixed for 3 minutes. Subsequently, water and superplasticizer were added, and the mixture was blended for 6 minutes. Finally, the materials were remixed for an additional 6 minutes to obtain the desired workability (Fig. 1).

Table 1. Material properties in the mixture employed to produce UHPC

Materials	Physical properties
Silica sand	Maximum diameter of sand: d ≤ 10mm
Cement	PCB40 ordinary Portland cement (Vietnamese standard)
Silica fume	SiO_2 content exceeding 98%
Superplasticizer	Polycarboxylic acid type and superplasticizer

(a) Standard sand

(b) Silica fume

(c) Cement

(d) calcined bauxite

(e) Silica powder, water, and superplasticizer

Fig. 2. Mixing material composition

Table 2. Mixture proportion used to produce UHPC

Cement (Type I)	Silica fume	Silica sand	Silica powder	Super-plasticizer	Water
1	0.25	1.1	0.3	0.067	0.2

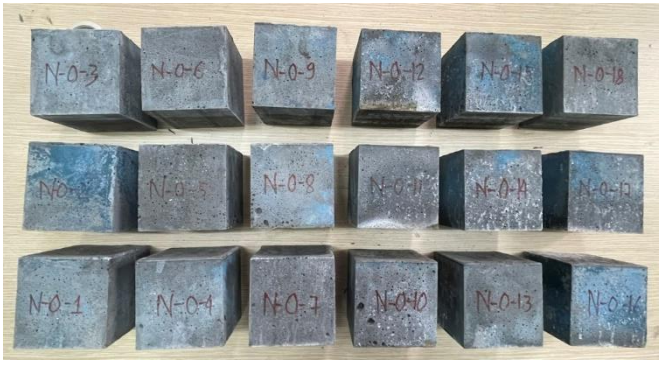

Fig. 3. Cube specimens for the case study of N-0

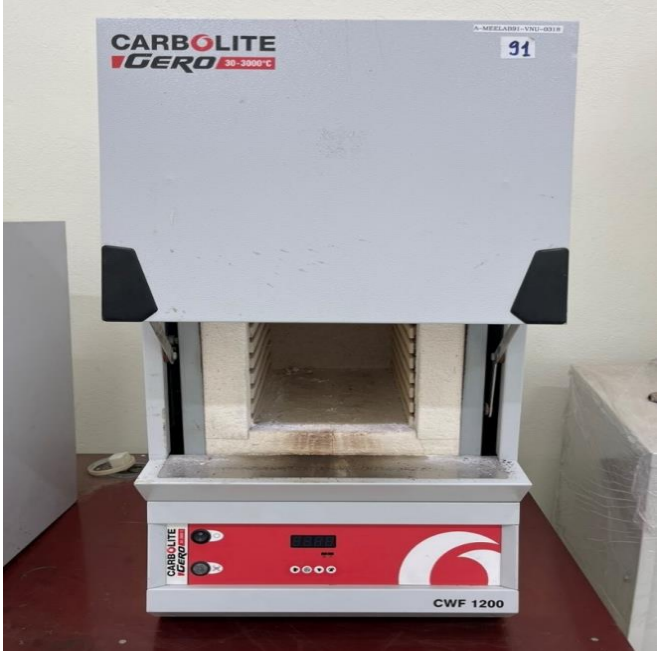

Fig. 4. Electrical Furnace for fire tests

In this study, calcined bauxite was considered a replacement for standard sand. A wide range of CB content, such as 0%, 20%, 40%, 60%, 80%, and 100%, was designed corresponding to six case studies denoted as N-0, N-I, N-II, N-II, N-IV, and N-V, respectively. 189 small-size

specimens (10 mm x 10 mm x 10 mm) were produced for the experiments in this study. Table 2 and Fig. 2 show the composition of the matrix mixture for UHPC specimens. It should be noted that 18 UHPC cube specimens are fabricated for each case study. Fig. 3 shows the 18 partial cube specimens for a case study of N-0. For spalling tests, three samples were tested for each thermal level, leading to a total of 72 specimens to be selected for the spalling test. These heated specimens are denoted as N-x-y-z, in which x is a case study; y is specimen number; and z is heating temperature. Furthermore, this study also considers the effects of chemical admixture, such as Sikament R7, Silkroad 1000, and Silkroad 5000P, corresponding to the case studies N-0-SR7, N-0-SK1000, and N-0-SK5000P.

Curing regimes

In this study, four types of curing methods consisting of ambient curing (AC) at $20℃$, $90℃$ hot-water curing (HWC), $90℃$ steam curing (ST), and $90℃$ air curing (90AC), are designed to characterize their influence on compressive strength of UHPC. In ambient curing, the specimens were put in a plastic box with water inside for 48 hours after casting and then de-mold and stored at 20℃ room temperature. Both 90℃ hot water and 90℃ air curing were conducted using a drying oven. It should be noted that all cube UHPC specimens are kept in the laboratory at ambient temperature for 28 days following the completion of all curing processes.

Explosive spalling tests

In this study, an electric furnace capable of reaching a maximum temperature of 1200 degrees Celsius was adopted to conduct the spalling tests with several thermal levels, such as 200°C, 400°C, and 600°C. Notably, the spalling behavior of UHPCs is highly sensitive to the heating rate, in which spalling behavior occurs within a narrow range of 1-10°C per minute. Therefore, the heating protocol carefully considers this sensitivity to ensure accurate observations. Therefore, the heating rate was set at 5°C/min. The specimens were subjected to three thermal levels as previously mentioned.

Mechanical test

In this study, mechanical properties of 28-day cube UHPC specimens can be obtained by employing an INSTRON 400HVL 2000 kN uniaxial compression equipment as seen in Fig. 5. The loading rate or strain rate for mechanical testing in this study was designed to be semi-static ($0.001s^{-1}$). It should be noted that at least five specimens were tested to obtain the average compressive strength. The cube UHPC specimens have a size of 100 mm width, 100 mm length, and 100 mm depth.

Fig. 5. INSTRON 400HVL 2000 kN testing machine

The heated specimens from the spalling experiments, which were exposed to elevated temperatures (i.e. 200°C, 400°C, and 600°C), were then subjected to the uniaxial compressive testing to determine the residual compressive strength of UHPC. It is important to note that these heated specimens were stored at room temperature for 7 days before mechanical testing. Due to the time-consuming spalling tests, a minimum of three heated UHPC specimens are tested. The input parameters and equipment used for this experiment were identical to those used for testing the unheated UHPC specimens.

Fig. 6. Scanning Electron Microscope machine for observing the microstructural evolution

Microstructural tests

A scanning electron microscope (SEM) was utilized to observe the microstructural evolution as well as discover the relationship between the spalling behavior and residual mechanical properties. The SEM specimens used for the microstructural examination can be selected from the cube UHPC specimens and were then immersed in isopropyl alcohol and dried in an oven at 60°C for 24 hours before the examination. Furthermore, energy-dispersive X-ray spectroscopy (EDS) analysis was conducted to identify the microstructural components in the UHPC matrix. The machine used for the microstructural test is shown in Fig. 6.

3. Results and Discussion

Optimal mixing composition and curing regimes

In this study, one of the objectives is to optimize the material composition used for UHPC mixing. First of all, two types of sand have been selected, such as yellow river sand and ISO standard sand as shown in Fig. 7. Both types of sand were then used to produce the cube UHPC specimens with the same mixture proportion (Table 2) and the same mixing procedure (Fig. 1). At least 9 specimens were produced and then maintained in the ambient condition for 48 hours after that 90℃ steam curing was applied for these specimens. Consequently, the uniaxial compressive tests were conducted to obtain the 14-day compressive strength and the comparison of compressive strength values of UHPC using yellow river and standard sands were illustrated in Fig. 8a. As seen, the UHPC specimens with yellow river sand provide low-compressive strength than the specimens with ISO standard sand. Indeed, ISO standard sand cube specimens provide an average value of 93.18 MPa while the value of 65.44 MPa was obtained for the specimens using yellow river sand. Based on this comparison, the ISO stand sand was recommended for the case study in this research.

a) Yellow river sand b) ISO standard sand

Fig. 7. Comparison of morphology of sand

Another mixture proportion examined in this study is the superplasticizer. Consequently, three types of superplasticizers were employed: Sikament R7, Silkroad 1000, and Sikroand 5000-P. The same mixture proportion (as detailed in Table 1) was applied to produce the cube UHPC specimen. The specimens using Sikament R7, Silkroad 1000, and Sikroand 5000-P were denoted

as N-0-SR7, N-0-SK1000, and N-0-SK5000P, respectively. Consequently, these UHPC specimens were produced using the procedure in Fig. 1 and the uniaxial compressive experiments were conducted on these cube UHPC specimens to investigate the effects of chemical admixtures on the compressive strength of UHPC. The comparison shown in Fig. 8b indicated that the 14-day compressive strength of N-0-SR7, which is an average value obtained from 6 cube UHPC specimens, is 69.78 ± 5.48 MPa while the UHPC specimens using Silkroad 1000 (N-0-SK1000) produce 60.87 ± 6.23 MPa. Additionally, the cube UHPC specimens using Sikroand 5000-P (N-0-SK5000P) can generate a compressive strength of 93.18 ± 4.71 MPa. The experimental results indicated that Silkroad5000P can generate the highest compressive strength of cube UHPC specimens, and Silkroad1000 UHPC specimens provide the lowest compressive strength. This comparison confirms that the Silkroad5000-P was suggested for the mixing composition in this study to generate higher strength. Therefore, the mixture compositions of UHPC were designed in this study as illustrated in Table 3.

Table 3. Mixture proportions of the UHPC (unit: kg/m3)

Cement	Silica fume	Standard sand	Silica powder	Water	Silkroad 5000-P
857	214	943	257	171	57

Another issue that need to be clarified is the curing regimes for cube UHPC specimens. In this study, several types of curing regimes were applied, such as ambient curing (N-0-AC), $90℃$ hot water curing (N-0-HWC), $90℃$ hot air curing (N-0-90AC), and $90℃$ steam curing (N-0-ST) as mentioned in the previous section. The mixture proportions of UHPC in Table 3 were applied to produce all UHPC specimens and these specimens were then maintained using four curing methodologies. Consequently, these specimens were tested using the uniaxial compressive experiment to obtain the corresponding compressive strength of materials and the results were presented in Fig. 8c. It can be observed that the 14-day compressive strength of N-0-AC provides 75.94 ± 7.25 MPa while the hot water curing exhibits the average values of 83.89 ± 4.81 MPa. Using $90℃$ hot air curing can generate a compressive strength of 89.43 ± 4.0 MPa, especially the cube UHPC can reach 93.18 ± 4.71 MPa when applying $90℃$ steam curing method. This means that $90℃$ steam curing method can generate the highest values of compressive strength at the same condition. Therefore, stream curing is recommended for application in the case study's subsequent steps.

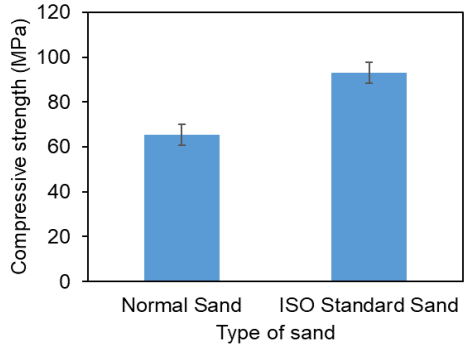

a) Effects of different types of sand on compressive strength

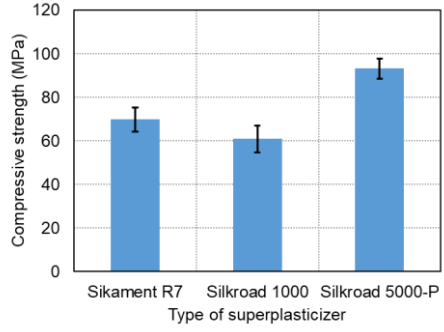

b) Effects of superplasticizer types on compressive strength

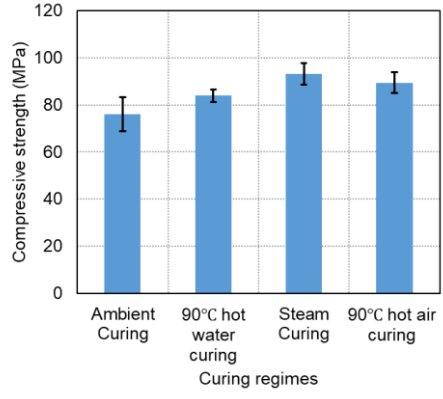

c) Effects of curing methods on compressive strength

Fig. 8. Optimal mixing composition for UHPC

Microstructural evolution under thermal conditions and CB content

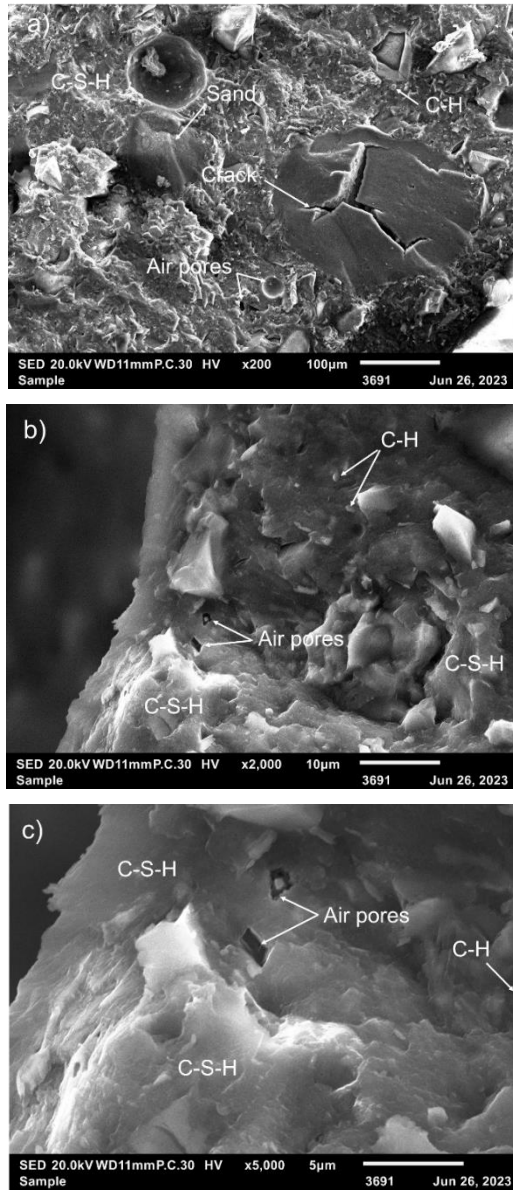

Fig. 9. Microstructural evolution under ambient temperature for the case of N-I

The reduction in mechanical properties of UHPC under thermal conditions can be attributed to the microstructural changes that occur when the concrete is exposed to high temperatures [17]. Figs. 9, 10, 11, and 12 present the SEM analysis of UHPC exposed to temperatures ranging from 20°C to 600°C, conducted using a JEOL JSM-IT210 scanning electron microscope. In the case of N-I, the microstructure at 20°C consists of scattered calcium hydroxide (C-H) phases and a continuous, compact calcium silicate hydrate (C-S-H) gel as seen in Fig. 9. Air pores and micro-cracks are also present. At this thermal level, the microstructure of UHPC exhibited that the continuous and compact C-S-H phase is predominant. When the thermal increases to 200°C, the C-H phase decreases in both quantity and size, while the C-S-H phase remains continuous and becomes more compact as observed in Fig. 10. At 400°C, the C-S-H phase exhibits an even more compact structure and improved integrity, while the C-H phase continues to diminish. At this temperature, the C-H phase is difficult to distinguish within the microstructure. Additionally, Figure 11 shows the emergence of needle-like C-S-H phases at high temperatures; however, these are less prevalent and not dominant.

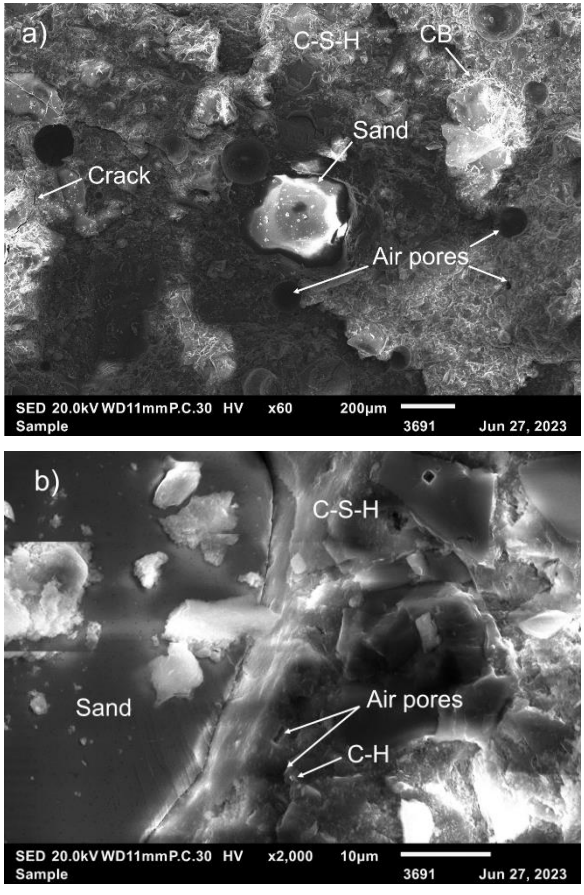

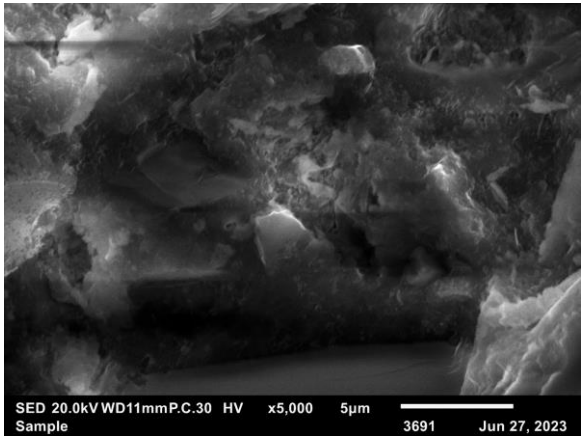

Fig. 10. Microstructural evolution at 200℃ for the case of N-I

When the temperature reaches 600℃, the microstructure is damaged more seriously as illustrated in Fig. 12. It can be observed that the micro-cracks and air-pores occur more frequently, whereas the C-H phase seems to disappear. At this thermal level, the C-S-H gel decomposed leading to the formation of needle-like C-S-H gel, which can be observed more frequently compared with the lower thermal levels. The presence of micro-cracks and needle-like C-S-H gel in the microstructure of UHPC at 600℃ may lead to the degradation of mechanical properties.

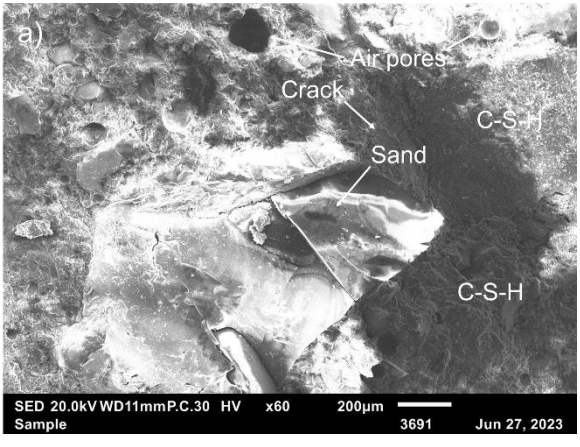

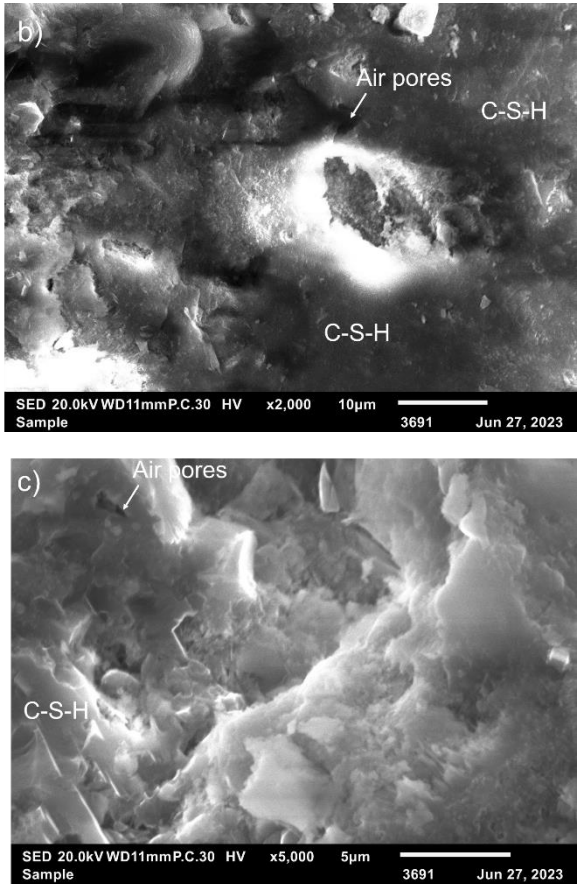

Fig. 11. Microstructural evolution at 400℃ for the case of N-I

As previously mentioned, calcined bauxite was added to the mixture in this study to enhance the fire resistance and reduce spalling behavior in UHPC. Therefore, the influences of CB content on the microstructure of UHPC at **400**℃ were presented in Fig. 13. As seen, the CB content plays an important role in the microstructural evolution. For specimens without CB content (N-0), the C-S-H phase exhibits a less compact and continuous structure, furthermore, the needle-like C-S-H gel can be observed more frequently. For the case of N-I (20% CB content), C-H phase completely decomposed and the C-S-H gel showed a good continuous and compact structure. Needle-like C-S-H gel could be observed; however, the quantity of this phase is limited. The C-S-H gel was still predominant. With 100% CB content, a continuous and compact C-S-H gel was well formed as seen in Fig. 13c. The needle-like C-S-H gel was not found in the microstructure of UHPC. This may lead to higher residual compressive strength of UHPC

compared with those for the specimen without CB content. The effects of CB content on residual compressive strength of UHPC subjected to thermal conditions are presented in the next section.

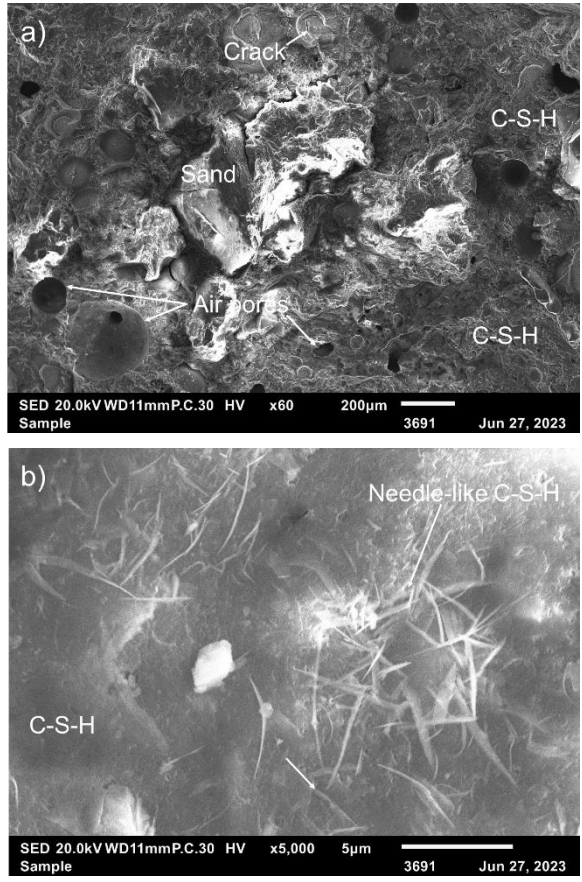

Fig. 12. Microstructural evolution at 600℃ for the case of N-I

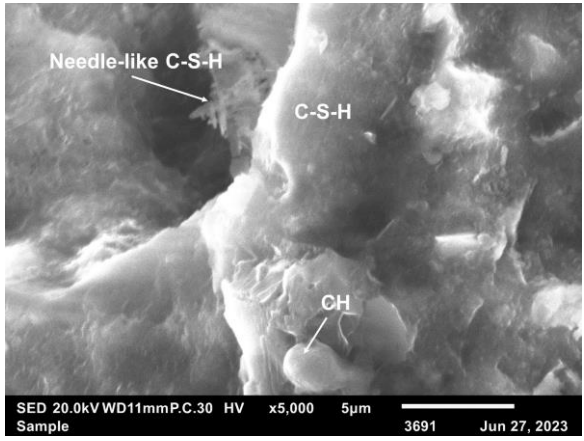

a) Microstructural evolution of N-0

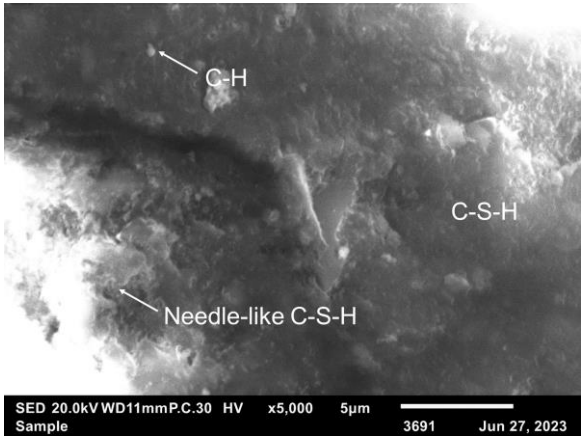

b) Microstructural evolution of N-I

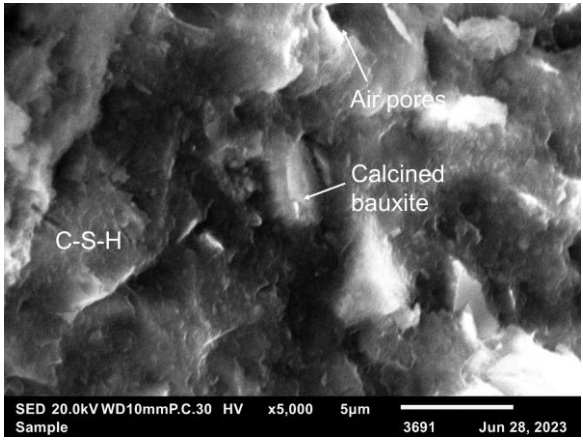

c) Microstructural evolution of N-V

Fig. 13. The influence of CB content on microstructural evolution at 400℃

Influences of CB content to residual compressive strength of UHPC

The thermal condition and CB content affected not only the microstructural evolution but also the degradation of the mechanical properties of UHPC. To clarify the influences of CB content on the residual compressive strength, mechanical tests were conducted on the heated specimens to determine the residual compressive strength, and the results are shown in Fig. 14.

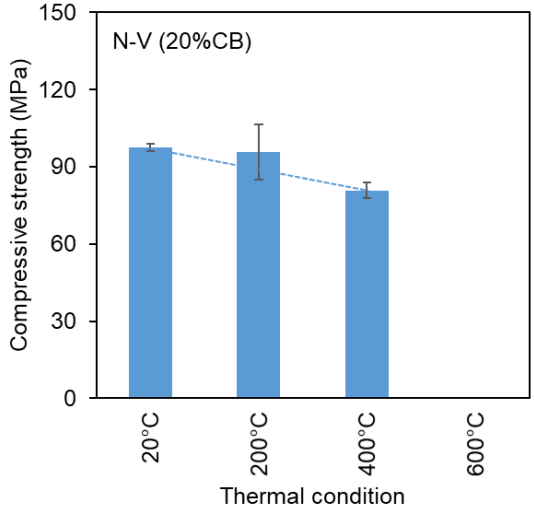

a) Variation of compressive strength of UHPC with 20% CB content

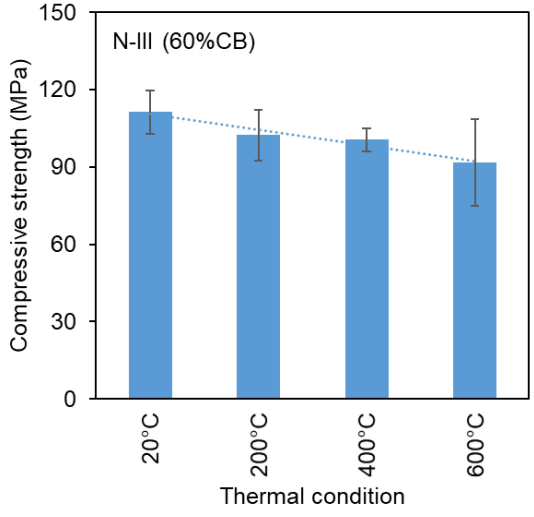

b) Variation of compressive strength of UHPC with 60% CB content

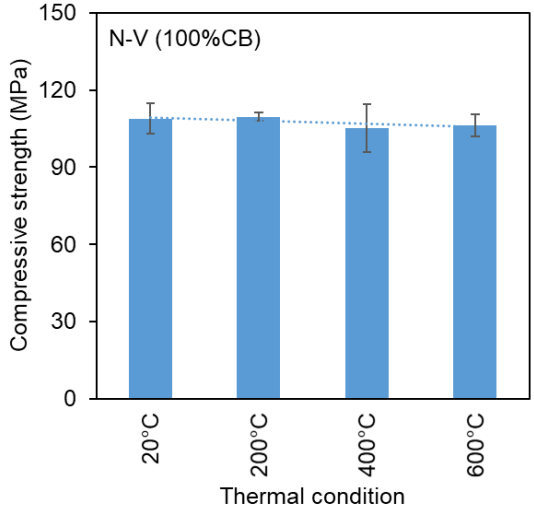

c) Variation of compressive strength of UHPC with 100% CB content

Fig. 14. Influences of CB content on residual compressive strength of UHPC at 400℃

The results indicated that both thermal condition and CB content significantly influences the remaining capacity of concrete at 400℃. For the most cases, when the temperature increases from 20℃ to 200℃, the residual compressive strength seems to unchanged. The reason for this phenomenon lies in the C-S-H gel becoming more continuous and compact structure in this temperature range as observed in Figs. 9-12, whereas the C-H phase partially decomposes and becomes smaller. When the temperature reaches 400℃, the effects of CB content on compressive strength are more pronounced. For the case of 20% CB content (N-I), the C-H completely decomposed and the formation of needle-like C-S-H gel was observed, resulting in a dramatic decrease of compressive strength as seen in Fig. 14a. When the CB content increases to 60% (N-III), the influences of thermal condition to compressive strength gradually decreases. These effects become less pronounced when the CB content reaches to 100% (N-V). The compact C-S-H gel is well-formed, as shown in Fig. 13c, whereas needle-like C-S-H gel is absent from the UHPC microstructure, which contributes to the enhanced residual compressive strength. The experimental results in this study indicated that the CB content played an important role in enhancing the fire resistance of UHPC.

4. Conclusions

This study investigated the effects of calcined bauxite (CB) content on the residual compressive strength and microstructural evolution of UHPC through uniaxial compression, spalling tests,

and scanning electron microscopy examination. The results indicated that at ambient temperature, UHPC's microstructure consists of dispersed C-H phases in a continuous, compact C-S-H matrix. Heating to 200°C reduces the quantity and size of C-H phases while making the C-S-H phase more compact. At 400°C, the C-S-H phase partially decomposes, with fewer C-H phases and the appearance of sparse needle-like C-S-H phases. At 600°C, UHPC shows significant microstructural damage, with increased micro-cracks and air pores, disappearance of C-H phases, and more prevalent needle-like C-S-H phases, leading to mechanical property degradation. CB content significantly enhances UHPC's fire resistance. At 20% CB content, complete C-H decomposition and needle-like C-S-H formation occur, greatly reducing compressive strength. As CB content increases to 60%, the thermal impact on compressive strength lessens. At 100% CB content, these effects are minimal, with a well-formed, compact C-S-H gel and no needle-like C-S-H phases, enhancing residual compressive strength.

Acknowledgment

Nguyen Ngoc Vinh acknowledges the project for the enhancement of education, research, and university management capacity at Vietnam-Japan University Research Grant Program of Japan International Cooperation Agency (JICA)

WORKS CITED

D.Y. Yoo, Y.S. Yoon, A Review on Structural Behavior, Design, and Application of Ultra-High-Performance Fiber-Reinforced Concrete, Int. J. Concr. Struct. Mater. 10 (2016) 125–142. https://doi.org/10.1007/s40069-016-0143-x.

X. Hou, S. Cao, Q. Rong, W. Zheng, G. Li, Effects of steel fiber and strain rate on the dynamic compressive stress-strain relationship in reactive powder concrete, Constr. Build. Mater. 170 (2018) 570–581. https://doi.org/10.1016/j.conbuildmat.2018.03.101.

P.A. Sarmiento, B. Torres, D.M. Ruiz, Y.A. Alvarado, I. Gasch, A.F. Machuca, Cyclic behavior of ultra-high performance fiber reinforced concrete beam-column joint, Struct. Concr. 20 (2019) 348–360. https://doi.org/10.1002/suco.201800025.

C. Shi, Z. Wu, J. Xiao, D. Wang, Z. Huang, Z. Fang, A review on ultra high performance concrete: Part I. Raw materials and mixture design, Constr. Build. Mater. 101 (2015) 741–751. https://doi.org/10.1016/j.conbuildmat.2015.10.088.

D. Wang, C. Shi, Z. Wu, J. Xiao, Z. Huang, Z. Fang, A review on ultra high performance concrete: Part II. Hydration, microstructure and properties, Constr. Build. Mater. 96 (2015) 368–377. https://doi.org/10.1016/j.conbuildmat.2015.08.095.

J. Liu, J. Wei, J. Li, Y. Su, C. Wu, A comprehensive review of ultra-high performance concrete (UHPC) behaviour under blast loads, Cem. Concr. Compos. 148 (2024). https://doi.org/10.1016/j.cemconcomp.2024.105449.

M.L. da Silva, L.P. Prado, E.F. Félix, A.M.D. de Sousa, D.P. Aquino, The Influence of Materials on the Mechanical Properties of Ultra-High-Performance Concrete (UHPC): A Literature Review, Materials (Basel). 17 (2024). https://doi.org/10.3390/ma17081801.

B.A. Graybeal, R.G. El-Helou, Structural Design with Ultra-High Performance Concrete, Fhwa-Hrt-23-077. (2023).

R. Ullah, Y. Qiang, J. Ahmad, N.I. Vatin, M.A. El-shorbagy, Ultra-High-Performance Concrete (UHPC):, (2022) 1–27.

M. Amran, G. Murali, N. Makul, M. Kurpińska, M.L. Nehdi, Fire-induced spalling of ultra-high performance concrete: A systematic critical review, Constr. Build. Mater. 373 (2023). https://doi.org/10.1016/j.conbuildmat.2023.130869.

F.P. Figueiredo, A.H. Shah, S.S. Huang, H. Angelakopoulos, K. Pilakoutas, I. Burgess, Fire Protection of Concrete Tunnel Linings with Waste Tyre Fibres, Procedia Eng. 210 (2017) 472–478. https://doi.org/10.1016/j.proeng.2017.11.103.

F.P. Figueiredo, S.S. Huang, H. Angelakopoulos, K. Pilakoutas, I. Burgess, Effects of Recycled Steel and Polymer Fibres on Explosive Fire Spalling of Concrete, Fire Technol. 55 (2019) 1495–1516. https://doi.org/10.1007/s10694-019-00817-9.

X. Hou, P. Ren, Q. Rong, W. Zheng, Y. Zhan, Comparative fire behavior of reinforced RPC and NSC simply supported beams, Eng. Struct. 185 (2019) 122–140. https://doi.org/10.1016/j.engstruct.2019.01.097.

L. Missemer, E. Ouedraogo, Y. Malecot, C. Clergue, D. Rogat, Fire spalling of ultra-high performance concrete: From a global analysis to microstructure investigations, Cem. Concr. Res. 115 (2019) 207–219. https://doi.org/10.1016/j.cemconres.2018.10.005.

H. Qin, J. Yang, K. Yan, J.H. Doh, K. Wang, X. Zhang, Experimental research on the spalling behaviour of ultra-high performance concrete under fire conditions, Constr. Build. Mater. 303 (2021) 124464. https://doi.org/10.1016/j.conbuildmat.2021.124464.

Y. Du, H.H. Qi, S.S. Huang, J.Y. Richard Liew, Experimental study on the spalling behaviour of ultra-high strength concrete in fire, Constr. Build. Mater. 258 (2020) 120334. https://doi.org/10.1016/j.conbuildmat.2020.120334.

S. Banerji, V. Kodur, Effect of temperature on mechanical properties of ultra-high performance concrete, Fire Mater. 46 (2022) 287–301. https://doi.org/10.1002/fam.2979.

D. Zhang, Y. Liu, K.H. Tan, Spalling resistance and mechanical properties of strain-hardening ultra-high performance concrete at elevated temperature, Constr. Build. Mater. 266 (2021) 120961. https://doi.org/10.1016/j.conbuildmat.2020.120961.

Y. Li, D. Zhang, Effect of lateral restraint and inclusion of polypropylene and steel fibers on spalling behavior, pore pressure, and thermal stress in ultra-high-performance concrete (UHPC) at elevated temperature, Constr. Build. Mater. 271 (2021). https://doi.org/10.1016/j.conbuildmat.2020.121879.

B. Guan, A. Wang, H. Zhao, J. Liu, X. Xue, H. Qiu, L. Li, Laboratory evaluation of microwave heating and skid resistance of pavement friction surfacing using calcined bauxite and magnetite aggregates, Constr. Build. Mater. 384 (2023) 131436. https://doi.org/10.1016/j.conbuildmat.2023.131436.

M.F. Zawrah, Effect of zircon additions on low and ultra-low cement alumina and bauxite castables, Ceram. Int. 33 (2007) 751–759. https://doi.org/10.1016/j.ceramint.2005.12.019.

S. Li, R. Xiong, X. Dong, Y. Sheng, B. Guan, Y. Zong, C. Xie, J. Zhai, C. Li, Effect of chemical composition of calcined bauxite aggregates on mechanical and physical properties for high friction surface course, Constr. Build. Mater. 302 (2021) 124390. https://doi.org/10.1016/j.conbuildmat.2021.124390.

J. Ye, W. Zhang, D. Shi, Effect of elevated temperature on the properties of geopolymer synthesized from calcined ore-dressing tailing of bauxite and ground-granulated blast furnace slag, Constr. Build. Mater. 69 (2014) 41–48. https://doi.org/10.1016/j.conbuildmat.2014.07.002.

R. Zhong, F. Zhang, Engineering high-performance cementitious matrices for improved projectile impact resistance with silane, micro fibrillated cellulose and fine calcined bauxite aggregate, Cem. Concr. Compos. 135 (2023) 104835. https://doi.org/10.1016/j.cemconcomp.2022.104835.

S.H. Park, D.J. Kim, S.W. Kim, Investigating the impact resistance of ultra-high-performance fiber-reinforced concrete using an improved strain energy impact test machine, Constr. Build. Mater. 125 (2016) 145–159. https://doi.org/10.1016/j.conbuildmat.2016.08.027.

D.J. Kim, S. El-Tawil, A.E. Naaman, Rate-dependent tensile behavior of high performance fiber reinforced cementitious composites, Mater. Struct. Constr. 42 (2009) 399–414. https://doi.org/10.1617/s11527-008-9390-x.

N.T. Tran, T.K. Tran, D.J. Kim, High rate response of ultra-high-performance fiber-reinforced concretes under direct tension, Cem. Concr. Res. J. 69 (2015) 72–87. https://doi.org/10.1016/j.cemconres.2014.12.008.